

Estimation of neutron star mass and radius of FRB 20240114A by identification of crustal oscillations

HAJIME SOTANI ,^{1,2,3} Z. WADIASINGH ,^{4,5,6} AND C. CHIRENTI ,^{4,5,6}

¹Department of Mathematics and Physics, Kochi University, Kochi, 780-8520, Japan

²RIKEN Center for Interdisciplinary Theoretical and Mathematical Sciences (iTHEMS), RIKEN, Wako 351-0198, Japan

³Theoretical Astrophysics, IAAT, University of Tübingen, 72076 Tübingen, Germany

⁴Department of Astronomy, University of Maryland, College Park, MD 20742-2421, USA

⁵Astrophysics Science Division, NASA Goddard Space Flight Center, Greenbelt, MD 20771, USA

⁶Center for Research and Exploration in Space Science and Technology, NASA/GSFC, Greenbelt, MD 20771, USA

ABSTRACT

By identifying quasi-periodic oscillations (QPOs) reported in FRB 20240114A (from the Five-hundred-meter Aperture Spherical Telescope) with neutron star crustal torsional oscillations, together with experimental constraints on the incompressibility K_0 of symmetric nuclear matter at saturation density, we constrain the mass and radius of an extragalactic neutron star at redshift $z \approx 0.13$. Identifying the low-order QPO frequencies as fundamental oscillations, and frequencies of 567.7 Hz or 655.5 Hz (rest frame) as first overtone candidates, implies neutron star mass ranges of $1.00\text{--}1.55 M_{\odot}$ or $1.17\text{--}1.76 M_{\odot}$, respectively. The radius is also constrained, with a self-consistent value around 13 km, further supported by the calculation of the NS structure within the low-mass/low-central density regime. Simultaneously, we also constrain another nuclear saturation parameter, namely the density dependence of the nuclear symmetry energy at saturation density (i.e., the slope parameter), L , and determine it to be $L = 59.5\text{--}96.8$ MeV with $\sim 10\%$ systematic uncertainty, which is broadly consistent with previous constraints on L obtained from experiments and astronomical observations. Thus, a mapping of FRB QPOs to crustal torsional modes seems reasonable. This can be confirmed with upcoming FRB surveys over a broad range of redshifts and more elaborate data analyses.

1. INTRODUCTION

Fast radio bursts (FRBs, I. R. Linscott & J. W. Erkes 1980; D. R. Lorimer et al. 2007; D. Thornton et al. 2013; F. Crawford et al. 2022; D. R. Lorimer et al. 2024) are energetic radio phenomena with rest-frame durations ranging from microseconds to several milliseconds. Most are extragalactic, with activity levels ranging from single bursts to thousands of repeat bursts from an individual source (E. Petroff et al. 2019; M. Caleb & E. Keane 2021). Their origins and mechanisms are still uncertain with many proposed models (e.g., E. Platts et al. 2019; D. Xiao et al. 2021; G. Voisin 2021; B. Zhang 2023). Magnetized neutron stars (NSs), particularly magnetars, are leading engine candidates. However, even magnetar models have a range of proposed emission locales, physical mechanisms, triggers, and source conditions. Most early models invoked magnetar giant flares with FRB generation and escape taking place at large distances in shocks (e.g., S. B. Popov & K. A. Postnov 2010; Y. Lyubarsky 2014; A. M. Beloborodov 2017; B. D. Metzger et al. 2019; A. M. Beloborodov 2020). However, shock models with ‘hyperactive’ young magnetars suffer from low efficiency and inability to explain short timescale microstructure (P. Beniamini & P. Kumar 2020), polarization jumps/swings (e.g., J. R. Niu et al. 2024; R. McKinven et al. 2025), or scintillation constraints (K. Nimmo et al. 2025). Magnetospheric magnetar models also range in physical conditions and mechanisms

(e.g., P. Kumar et al. 2017; W. Wang et al. 2018; Z. Wadiasingh & A. Timokhin 2019; A. G. Suvorov & K. D. Kokkotas 2019; Z. Wadiasingh et al. 2020; M. Lyutikov 2021; W.-Y. Wang et al. 2022). As already proposed prior to 2020, FRBs likely result from crust quakes and perturbations associated with magnetar short bursts (Z. Wadiasingh & A. Timokhin 2019; Z. Wadiasingh et al. 2020) where not all short bursts result in FRBs due to a threshold condition for the amplitude of crust perturbations. This is also consistent with lower-energy breaks observed in numerous individual repeating FRB luminosity/energy distributions (e.g., A. Kumar et al. 2025), i.e., a preferred energy scale for FRBs, and the earthquake-like statistics of some FRBs (T. Totani & Y. Tsuzuki 2023).

The magnetar engine for (at least some) FRBs was also empirically corroborated by the galactic event FRB 20200428A and its associated soft gamma-ray short burst, from magnetar SGR 1935+2154, in 2020 (CHIME/FRB Collaboration et al. 2020; C. D. Bochenek et al. 2020; S. Mereghetti et al. 2020; A. Ridnaia et al. 2021; C. K. Li et al. 2021; M. Tavani et al. 2021). This was preceded by thousands of magnetar short bursts with no observed FRB-like emission (G. Younes et al. 2020). More recently, during the outburst activity of SGR 1935+2154 in 2022 accompanied by short bursts, FRB-like bursts were temporally bracketed by two spin-up glitches (C.-P. Hu et al. 2024), the largest ever observed in NSs. This activity is also contemporaneous with

enhanced spin-down, along with rapid X-ray spectral evolution (C.-P. Hu et al. 2025), confirming some FRBs are the result of crustal activity with peculiar magnetospheric conditions.

A few percent of observed (extragalactic) FRBs contain sub-bursts or multipulse trains of bursts, separated by characteristic timescales of a few to tens of milliseconds (e.g., J. W. T. Hessels et al. 2019; Z. Pleunis et al. 2021). Additionally, repeater FRBs seem to universally feature a double-humped waiting time distribution (S. Yamasaki & T. Totani 2025), with no short-timescale periodicity (e.g., J.-R. Niu et al. 2022; S. Z. Sheikh et al. 2024; D. Zhou et al. 2025; J. I. Katz 2025). It was proposed in Z. Wadiasingh & A. Timokhin (2019) that the short-time hump is not simply microstructure but an imprint of engine-driven activity, i.e., the characteristic timescale of shear modes in the magnetar crust, and further expounded in Z. Wadiasingh & C. Chirenti (2020). Indeed, such a short-time hump is also seen in high-energy magnetar short bursts (D. Huppenkothen et al. 2015) along with quasi-periodic oscillations (QPOs) compatible with low-order fundamental crustal eigenmodes (D. Huppenkothen et al. 2014a,b). The lack of short timescale periodicity (associated with a more typical spin period of 1 – 10 s) results because the FRB engine could be an ultra-long period magnetar (Z. Wadiasingh et al. 2020; P. Beniamini et al. 2020, 2023; A. J. Cooper & Z. Wadiasingh 2024; A. V. Bilous et al. 2025; P. Beniamini & P. Kumar 2025; S. K. Lander et al. 2026). Long term polarimetric monitoring also seems to favor this picture (S. Bethapudi et al. 2025).

Remarkably, the HXMT-Insight hard X-ray component of FRB 20200428A also exhibits a $\sim 3.4\sigma$ QPO at ~ 40 Hz (X. Li et al. 2022), with a period compatible with the interval between radio peaks in FRB 20200428A. Thus, QPOs, if associated with crustal modes and perturbations, are likely capable of being imprinted on observed FRB interval times or substructure⁷. The interval spacing also disfavors strong beaming of emission, given the magnetar's spin. The FRB subpulses also led⁸ X-ray features by $\sim 2 - 3$ ms (U. Giri et al. 2023; M. Y. Ge et al. 2023), which is compatible with a gap Spitzer timescale (P. Beniamini et al. 2025) and is unexplained in shock or triggered reconnection models.

Thus, the close connection of FRB activity with NS crust physics, and identification⁹ of subpulse trains in FRBs with

⁷ The recent study by L. Burnaz et al. (2025) considered simulations of large-amplitude MHD-like waves in a force-free approximation for the imprinting of crust modes that may steepen into shocks or interact with upstream plasma. The background plasma (sourced by single-photon pair cascades) must exist to support such waves without charge starvation and/or being Compton thick, which is not a given, while also not inhibiting FRB escape. This contrasts with a low-twist magnetosphere with nearly vacuum-like conditions where crust perturbations drive pair creation and radio emission with a threshold condition.

⁸ See also C.-W. Wang et al. (2026) for FRB 20221014 from SGR 1935+2154 with similar lag.

⁹ We note that the imprinting mechanism proposed by L. Burnaz et al. (2025) arises from quake-driven elastic motions with a characteristic crust-crossing/bounce frequency (typically kHz in their model, well

possible coherent crustal modes rather than burst microstructure (e.g., M. Kramer et al. 2024) is supported by numerous pieces of evidence. We adopt this working hypothesis, which as demonstrated in the paper, yields results intriguingly consistent with a typical NS. Consistency is not enough to rule out alternatives to our hypothesis, but it can be tested against future (and imminent) large FRB samples from CHORD (K. Vanderlinde et al. 2019) and DSA (G. Hallinan et al. 2019; M. Sherman et al. 2024).

Examples of FRBs with reported QPO periods or clustering include FRB 20201020A (0.41 ms, I. Pastor-Marazuela et al. 2023), FRBs 20210206A and 20210213A (2.8 ms and 10.7 ms, respectively, CHIME/FRB Collaboration et al. 2022), FRB 20230708A (7.3 ms, T. Dial et al. 2025), FRB 20220912A (5.8 ms, S. Z. Sheikh et al. 2024), FRB 20190122C (1 ms, S. Xiao et al. 2026), and FRB 20121102A (22 ms, J. N. Jahns et al. 2023).

More recently, FRB 20240114A (K. Shin & CHIME/FRB Collaboration 2024) possesses an exceptionally large burst sample enabled by the Five-hundred-meter Aperture Spherical radio Telescope (FAST) (R. Nan et al. 2011; L.-X. Zhang et al. 2025) with numerous modest significance radio QPOs (D. Zhou et al. 2025). We choose to focus on this sample for this study. The reported QPO frequencies range from tens of Hz up to ~ 600 Hz, which are comparable to the QPOs discovered in X-rays from magnetar giant flares (e.g., T. E. Strohmayer & A. L. Watts 2005; A. L. Watts & T. E. Strohmayer 2006; T. E. Strohmayer & A. L. Watts 2006; A. L. Watts & T. E. Strohmayer 2007; M. C. Miller et al. 2019) and short bursts (D. Huppenkothen et al. 2014a,b).

NSs are astrophysical laboratories to probe the cold dense matter equation of state (EOS) (S. L. Shapiro & S. A. Teukolsky 1983). Because it is challenging to obtain information about nuclear properties at higher density regimes through terrestrial experiments, the EOS for NS matter is not yet fixed. NS observations and inferences offer a path. For instance, the discovery of massive NSs could exclude softer EOS models, with which the expected maximum mass does not reach the highest observed masses (P. B. Demorest et al. 2010; J. Antoniadis et al. 2013; H. T. Cromartie et al. 2020; E. Fonseca et al. 2021; R. W. Romani et al. 2022).

The oscillation frequencies of a NS also provide important information for extracting NS properties. Since the frequencies strongly depend on the interior properties of the NS, one may extract the NS properties by observing the frequencies (solving the inverse problem or, more appropriately, through forward modeling). This type of study is termed asteroseismology, in analogy to seismology on Earth and helioseismology on the Sun. Via future observations of these oscillation

above low-order fundamental torsional oscillation frequencies), coupled into force-free MHD magnetospheric disturbances. Low-order fundamental oscillations or magneto-elastic modes, as exhibited by FRB 20200428A and its associated short burst, seem also capable of being imprinted (Z. Wadiasingh & C. Chirenti 2020). Our approach instead tests whether the reported FRB QPOs can be mapped onto torsional-mode eigenfrequencies in simplified (non-magnetic) crust models.

frequencies in the gravitational waves from a NS, one may restrict the NS mass, radius, and EOS (e.g., [N. Andersson & K. D. Kokkotas 1996, 1998](#); [L. K. Tsui & P. T. Leung 2005](#); [H. Sotani et al. 2011](#); [D. D. Doneva et al. 2013](#)). This technique cannot yet be applied because gravitational wave detections of NS oscillation modes are not available, and magnetar QPOs therefore provide a practical alternative. In fact, by identifying the observed QPO frequencies with the crustal torsional oscillations, we can constrain the crust EOS and NS models (e.g., [M. Gearheart et al. 2011](#); [H. Sotani et al. 2012a](#); [Sotani, H. et al. 2023](#)).

Whereas the oscillation frequency associated with the dynamical time of a NS is on the order of a few kHz, the QPO frequencies observed from magnetars range from tens of Hz to kHz. Therefore, theoretical identification of these frequencies, especially lower than ~ 100 Hz, is more difficult. The potential candidates may be crustal torsional modes or magnetic oscillations (or magneto-elastic oscillations). However, the magnetic (and also magneto-elastic) oscillations strongly depend on magnetic geometry and distribution of magnetic field strength inside the star ([M. Gabler et al. 2013](#)), and also on how the magnetic fields are entangled (e.g., [B. Link & C. A. van Eysden 2016a,b](#); [J. Bretz et al. 2017, 2021](#)), all of which are still quite uncertain.

So, to avoid such uncertainties from the magnetic fields, we consider a simple description of crustal torsional oscillations without any magnetic effects in this study. We note that this assumption might be reasonable if the magnetic field is not extreme, because the modification of the frequencies of the crustal torsional oscillations becomes relevant for magnetic fields stronger than $\sim \text{few} \times 10^{15}$ G ([M. Gabler et al. 2018](#); [G. H. de Souza & C. Chirenti 2019](#); [Sotani, H. et al. 2023](#)). Torsional oscillations are axial-type oscillations, which do not involve radial motion. Namely, the shape of the star is not deformed by torsional oscillations.

There is a further advantage to identifying the QPOs with the crustal torsional oscillations. Since torsional oscillations are excited only inside the NS crust, where the elasticity becomes non-zero, EOS uncertainties in the core region have a minimum impact.¹⁰ As the QPOs discovered in FRB 20240114A also lie within the same frequency range as the magnetar QPOs, we propose to identify/map the QPOs observed in FRB 20240114A with crustal torsional oscillations and derive constraints on stellar models and EOS parameters ([H. Sotani et al. 2018](#); [Sotani, H. et al. 2023](#)).

This manuscript is organized as follows. In Sec. 2, we briefly review the specific frequencies observed in FRB 20240114A. In Sec. 3, we describe our NS models and the perturbation equations for the crustal torsional modes. Then, in Sec. 4, the NS model for FRB 20240114A is estimated by

¹⁰ Uncertainties in the unknown core EOS translate into uncertainties in the inferred core mass and radius. In our approach, we integrate the TOV equations inward from the surface to the crust-core boundary, so the resulting NS (crust) models are specified by two parameters, M and R . This contrasts with the standard outward integration from the center, where a fixed EOS yields a one-parameter family of stellar models.

Table 1. Lower-frequency QPOs: observed time interval between burst trains in FRB 20240114A, Δt_{ob} , and its statistical significance, as reported in Figs. 4 and D7 by [D. Zhou et al. \(2025\)](#). The observed frequency, ν_{ob} , estimated from Δt_{ob} , and the frequency in the rest-frame of the object, ν_0 , using Eq. (1), are also listed. The rightmost column is the corresponding value of ℓ , obtained by identifying the frequencies ν_0 with the ℓ -th fundamental frequencies of crustal torsional oscillations (see § 4.1 for details).

Δt_{ob} (ms)	significance (σ)	ν_{ob} (Hz)	ν_0 (Hz)	ℓ
13.3	3.0	75.2	85.0	10
30.6	3.2	32.7	36.9	4
48.8	3.0	20.5	23.2	3
62.6	3.9	16.0	18.1	2
5.5	1.8	181.8	205.6	> 13
11.5	1.6	87.0	98.3	11
14.7	2.2	68.0	76.9	9
21.4	1.9	46.7	52.8	6
25.7	2.6	38.9	44.0	5
29.5	2.8	33.9	38.3	4
44.8	1.5	22.3	25.2	3

identifying the observed frequencies with various ℓ -th fundamental frequencies and 1st overtone of crustal torsional oscillations, considering the experimental constraint on the incompressibility K_0 of symmetric nuclear matter at saturation density. Simultaneously, through the resultant stellar model for FRB 20240114A, we derive a constraint on the density dependence of the nuclear symmetry energy at saturation density, the slope parameter L . Finally, we summarize our findings in this study and the conclusions in Sec. 5. Unless otherwise mentioned, we adopt geometric units with $c = G = 1$, where c and G denote the speed of light and the gravitational constant, and use the metric signature $(-, +, +, +)$.

2. QUASI-PERIODIC OSCILLATIONS IN FRB 20240114A

FRB 20240114A is associated with a host galaxy at $z \approx 0.130287 \pm 0.000002$ ([J. Tian et al. 2024](#); [M. Bhardwaj et al. 2024](#); [X.-L. Chen et al. 2025](#); [G. Bruni et al. 2025](#); [M. Bhardwaj et al. 2025](#)). The reciprocal of the (quasi-)periodic time intervals between burst trains observed in FRB 20240114A using FAST ([D. Zhou et al. 2025](#)) provides an estimate of the lower quasiperiodic oscillation frequencies observed on Earth ($\lesssim 200$ Hz), ν_{ob} . The frequency observed in the rest-frame of the source, ν_0 , located at redshift z , is estimated by

$$\nu_0 = \nu_{\text{ob}}(1 + z), \quad (1)$$

([Z. Wadiasingh & C. Chirenti 2020](#)), as listed in Table 1.

D. Zhou et al. (2025) also report quasi-periodic oscillations in the few-hundred-Hz range for FRB 20240114A, presenting not only the central frequency, ν_{ob} , but also the full width at half maximum (FWHM_{ob}). From these, we can estimate the corresponding values observed in the source rest-frame, ν_0 and FWHM, via Eq. (1). Moreover, using ν_0 and FWHM, we can estimate the uncertainty in ν_0 (from the lack of precise wave phase information) as

$$\nu_{\text{min}} < \nu_0 < \nu_{\text{max}}, \quad (2)$$

where ν_{min} and ν_{max} are estimated from ν_0 and the frequency widths, $\Delta\nu$, (M. C. Miller et al. 2019) as

$$\nu_{\text{min}} = \nu_0 \left[1 - \frac{1}{2} \left(\frac{\Delta\nu}{\nu_0} \right)^2 \right], \quad (3)$$

$$\nu_{\text{max}} = \nu_0 \left[1 + \frac{1}{2} \left(\frac{\Delta\nu}{\nu_0} \right)^2 \right]. \quad (4)$$

In our case, $\Delta\nu$ is set to be half of the reported FWHM. The resulting values are listed in Table 2.

3. CRUSTAL TORSIONAL OSCILLATIONS

To calculate the crustal torsional oscillations, we first prepare the background NS models. We consider a static, spherically symmetric spacetime, whose metric is given by

$$ds^2 = -e^{2\Phi} dt^2 + e^{2\Lambda} dr^2 + r^2 d\theta^2 + r^2 \sin^2 \theta d\phi^2, \quad (5)$$

where the metric functions, Φ and Λ , depend only on the radial coordinate, r , and Λ is directly connected to the mass function, $m(r)$, as $e^{-2\Lambda} = 1 - 2m/r$. We construct our stellar models by integrating the TOV equations with an appropriate EOS for NS matter.

For any EOS, the bulk energy per nucleon can be expanded in the vicinity of the saturation density, n_0 , of symmetric nuclear matter at zero temperature (J. M. Lattimer 2012) as a function of the baryon number density, n_b , and neutron excess, α , given by $\alpha = (n_n - n_p)/(n_n + n_p)$ with the neutron and proton number densities, n_n and n_p , respectively:

$$w = w_0 + \frac{K_0}{18n_0^2} (n_b - n_0)^2 + \left[S_0 + \frac{L}{3n_0} (n_b - n_0) \right] \alpha^2, \quad (6)$$

where w_0 and K_0 are the saturation energy and incompressibility of symmetric nuclear matter at $n_b = n_0$, while the coefficient in the term with α^2 corresponds to the symmetry energy, $S(n_b)$. The symmetry energy is also expanded, as in Eq. (6), where S_0 and L are the symmetry energy and its density dependence at $n_b = n_0$, i.e., $S_0 = S(n_0)$ and $L = 3n_0 (dS/dn_b|_{n_b=n_0})$.

Among these five nuclear saturation parameters, n_0 , w_0 , and S_0 are relatively well constrained (M. Oertel et al. 2017; B.-A. Li et al. 2019), while the remaining two parameters, K_0 and L , are experimentally poorly constrained. This is because K_0 and L are the density derivatives at $n_b = n_0$,

but the experimental data are concentrated around saturation density. Nevertheless, experimental constraints on K_0 exist: $K_0 = 240 \pm 20$ MeV (S. Shlomo et al. 2006). Meanwhile, we adopt a fiducial $L = 60 \pm 20$ MeV (M. B. Tsang et al. 2012; Newton, William G. et al. 2014; B.-A. Li et al. 2019).

In order to systematically examine the torsional oscillations by changing the values of K_0 and L , we adopt the phenomenological EOS proposed by Oyamatsu and Iida (K. Oyamatsu & K. Iida 2003, 2007) (hereafter referred to as OI-EOSs) in this study. The OI-EOSs are constructed within the extended Thomas-Fermi theory in such a way that the bulk energy expression reduces to the expression given by Eq. (6) in the limit of $n_b \rightarrow n_0$ and $\alpha \rightarrow 0$, and that the values of n_0 , w_0 , and S_0 are optimized to reproduce experimental data for masses and charge radii of stable nuclei for given values of K_0 and L .

Crustal toroidal oscillations are restored by the elasticity of the crust, which is characterized by the shear modulus, μ . The shear modulus depends on the various phases of non-uniform nuclear structures. In the phase of body-centered cubic lattice of spherical nuclei, the effective shear modulus, μ_{sp} , has been derived as a function of nuclei number density, n_i , the charge number of nuclei, Z , and the radius of the Wigner-Seitz cell, a , as

$$\mu_{\text{sp}} = 0.1194 \frac{n_i(Ze)^2}{a} \quad (7)$$

under the assumption that the nuclei are point particles, and taking the average over all possible wave vectors of displacements (S. Ogata & S. Ichimaru 1990; T. Strohmayer et al. 1991) and $1/n_i = 4\pi a^3/3$.

It is theoretically suggested that non-spherical atomic nuclei, the so-called pasta structures, exist at the base of the crust, where the shape of the nuclei changes from spherical to cylindrical, slab-like, cylindrical-hole, and spherical-hole before matter becomes uniform, as density increases. The shear modulus in the phase of cylindrical nuclei is estimated as

$$\mu_{\text{cy}} = \frac{2}{3} E_{\text{Coul}} \times 10^{2.1(w_2 - 0.3)}, \quad (8)$$

where E_{Coul} and w_2 denote the Coulomb energy per volume of a Wigner-Seitz cell and the volume fraction of cylindrical nuclei. The shear modulus in slab-like nuclei is zero, at least to linear order (C. Pethick & A. Potekhin 1998). That is, matter in the phase of slab-like nuclei behaves as a fluid in the linear perturbation regime. In this study, we consider crustal torsional oscillations excited in the phases of spherical and cylindrical nuclei only. Although there is a possibility for additional excitation of torsional oscillations in the phases of cylindrical-hole and spherical-hole nuclei, they would be independent of the torsional oscillations we focus on (H. Sotani et al. 2019).

Additionally, the fraction of dripped neutrons in the crust that behave as a superfluid, i.e. the ratio of superfluid neutrons to dripped neutrons N_s/N_d , also modifies the frequencies of crustal torsional oscillations, as shown in H. Sotani et al. (2012b, 2013). Namely, the case with $N_s/N_d = 0$

Table 2. Higher-frequency QPOs: central frequency, ν_{ob} , the full width at half maximum (FWHM_{ob}), and quality factors (Q), reported for FRB 20240114A in Table 2 of [D. Zhou et al. \(2025\)](#). The QPO central frequency, ν_0 ; FWHM; and the minimum and maximum frequencies, ν_{min} and ν_{max} , using Eqs. (3) and (4), observed in the rest-frame of the object are also listed. The rightmost column is the corresponding value of (ℓ, n) , obtained by identifying the frequencies ν_0 with the ℓ -th frequencies of n -th overtone of the crustal torsional oscillations (see § 4.2 for details).

ν_{ob} (Hz)	FWHM _{ob} (Hz)	Q	ν_0 (Hz)	FWHM (Hz)	ν_{min} (Hz)	ν_{max} (Hz)	(ℓ, n)
266.85 ± 0.68	97.0 ± 1.3	2.750 ± 0.037	301.7 ± 0.8	106.7 ± 1.5	295.8	307.6	$(> 13, 0)$
502.1 ± 6.2	70.0 ± 14.0	7.10 ± 1.40	567.7 ± 7.0	79.1 ± 15.8	558.7	576.6	$(\ell, 1)$
327.94 ± 0.93	117.4 ± 1.7	2.793 ± 0.041	370.8 ± 1.05	132.7 ± 1.9	363.6	377.9	$(> 13, 0)$
579.8 ± 5.6	105.0 ± 10.0	5.50 ± 0.55	655.5 ± 6.3	118.7 ± 11.3	645.9	665.0	$(\ell, 1)$

is the situation in which all dripped neutrons comove with the nuclei, while the case with $N_s/N_d = 1$ is the situation in which all dripped neutrons behave as a superfluid and do not contribute to the torsional oscillations. The information on N_s/N_d is still poorly understood, but it is estimated in the phase of spherical nuclei by [N. Chamel \(2012\)](#), which depends on the density, and we adopt this estimation in this study. Meanwhile, since the value of N_s/N_d inside the phase of cylindrical nuclei is poorly understood, we consider the extreme cases with $N_s/N_d = 0$ and 1 for this phase.

The perturbation equation for crustal torsional oscillations is derived by linearizing the equation of motion and can be written as:

$$\mathcal{Y}'' + \left[\left(\frac{4}{r} + \Phi' - \Lambda' \right) + \frac{\mu'}{\mu} \right] \mathcal{Y}' + \left[\frac{\tilde{H}}{\mu} \omega^2 e^{-2\Phi} - \frac{(\ell+2)(\ell-1)}{r^2} \right] e^{2\Lambda} \mathcal{Y} = 0, \quad (9)$$

where \mathcal{Y} denotes the radial dependence of the angular displacement, and the prime denotes the derivative with respect to r , \tilde{H} is the effective enthalpy density defined below, and ω denotes the angular frequency of the ℓ -th torsional oscillations ([B. L. Schumaker & K. S. Thorne 1983](#); [H. Sotani et al. 2012b, 2013](#)). \tilde{H} depends on the value of N_s/N_d as $\tilde{H} = (1 - N_s/A)H$, where A denotes the baryon number inside a Wigner-Seitz cell and H is the total enthalpy given by $H = \varepsilon + p$, where ε is the total energy density, and p is the fluid pressure. The boundary conditions to solve this equation are the vanishing of the traction force at the base and at the top of the crust, which reduce to $\mathcal{Y}' = 0$ at these points ([B. L. Schumaker & K. S. Thorne 1983](#); [H. Sotani et al. 2007](#)). We note that one can determine not only the fundamental frequencies but also the overtones by solving the eigenvalue problem of Eq. (9), imposing the same boundary conditions.

4. ESTIMATING A NEUTRON STAR MODEL FOR FRB 20240114A

4.1. Fundamental Torsional Oscillations

For a given NS model, with a specified mass, radius, N_s/N_d , and EOS parameters K_0 and L , the frequencies of

the torsional oscillations are fully determined. However, it has been shown that the frequencies of the ℓ -th fundamental torsional oscillations depend only weakly on K_0 and can therefore be characterized as a function of L as

$$\ell t_0 \text{ (Hz)} = c_{\ell}^{(0)} + c_{\ell}^{(1)} L_{100}^{1/2} + c_{\ell}^{(2)} L_{100} + c_{\ell}^{(3)} L_{100}^2, \quad (10)$$

where L_{100} is defined as $L_{100} \equiv L/(100 \text{ MeV})$ and $c_{\ell}^{(i)}$ for $i = 0, 1, 2, 3$ are fitting parameters that depend on the mass, radius, and N_s/N_d ([H. Sotani et al. 2012a,b, 2013](#))¹¹. In Fig. 1 we show the correspondence between the QPO frequencies, ν_0 , listed in Table 1, and the frequencies of fundamental torsional oscillations with specific values of ℓ , calculated as a function of L for the stellar model with $1.4M_{\odot}$ and 12 km. The solid (dashed) horizontal lines denote ν_0 whose reported statistical significance is larger than or equal to (smaller than) 3σ . The upper and lower panels correspond to the results with $N_s/N_d = 0$ and 1, respectively, and the coefficients in Eq. (10) are listed in Table 3. Each QPO frequency in Table 1 can be consistently identified with one of the ℓ -th crustal torsional modes and the corresponding values of ℓ are also listed in Table 1. The only exception is the 205.6 Hz QPO, which might be identified with a very high ℓ fundamental mode.

Since the QPO frequencies reported in Table 1 are estimated from the time interval between the FRB burst trains, the lower limit in the uncertainty on Δt_{ob} is at the scale of the radio pulse widths, τ . As that is not readily available, we (conservatively) adopt a uniform uncertainty in τ . Then, ν_{ob} is estimated as

$$\Delta\nu_{\text{ob}} \simeq \nu_{\text{ob}}^2 \tau. \quad (11)$$

This choice gives more statistical weight to low-frequency QPOs, i.e., well-separated trains where the putative mode's period spacing between each ℓ is larger and identification is less ambiguous. We then propagate the uncertainty to the rest-frame of the object, $\Delta\nu_0$, as

$$\Delta\nu_0 = \Delta\nu_{\text{ob}}(1+z) \simeq \nu_{\text{ob}}^2(1+z)\tau. \quad (12)$$

¹¹ Here, we include an additional $L_{100}^{1/2}$ term in the function of L for the fundamental frequencies (10) for greater accuracy.

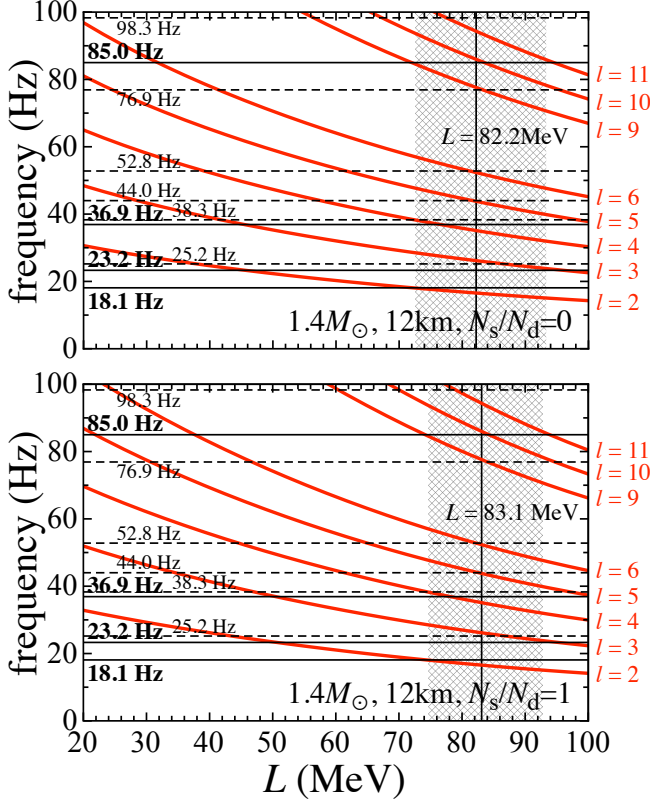


Figure 1. The rest-frame frequencies, ν_0 , listed in Table 1 (except for 205.6 Hz), identified with the fundamental frequencies of crustal torsional oscillations with various values of ℓ , for the NS model with $1.4M_\odot$ and 12 km. The top and bottom panels correspond to the results with $N_s/N_d = 0$ and 1, respectively. The horizontal solid lines with the QPO frequencies written in bold font are frequencies with statistical significance greater than or equal to 3σ , while the dashed lines with the QPO frequencies written in thin font are those with significance less than 3σ . The vertical lines denote the optimal value of L to identify the QPO frequencies with the fundamental frequencies of the crustal torsional oscillations, while the shaded regions denote $L \pm 1\sigma$.

Here, we conservatively adopt $\tau \equiv 3$ ms to estimate $\Delta\nu_0$. This value is approximately the reported median of the effective pulse widths for FRB 20240114A with FAST (L.-X. Zhang et al. 2025), and under our assumptions, is a systematic uncertainty associated with the times-of-arrival of a train of pulses within the radio burst. The reported precision of the times-of-arrival of the pulses is considerably better than $\tau = 3$ ms, however for broadened pulses (by choice of dispersion measure optimizing scheme, for instance), the intervals between observed peaks of pulses may not precisely map to the underlying physical mode. A future analysis could improve upon these assumptions by using morphological in-

Table 3. Coefficients in Eq. (10) for the fundamental modes with specific values of ℓ and for the NS model shown in Fig. 1.

N_s/N_d	ℓ	$c_\ell^{(0)}$	$c_\ell^{(1)}$	$c_\ell^{(2)}$	$c_\ell^{(3)}$
0	2	44.07	-26.94	-7.979	5.131
	3	69.68	-42.58	-12.65	8.125
	4	93.47	-57.08	-17.01	10.91
	5	116.6	-71.15	-21.24	13.61
	6	139.3	-84.94	-25.48	16.28
	9	206.4	-125.3	-38.45	24.30
	10	228.6	-138.6	-42.81	26.97
	11	250.7	-151.7	-47.33	29.67
1	2	44.86	-17.49	-22.87	9.619
	3	70.89	-27.52	-36.30	15.24
	4	95.08	-36.88	-48.71	20.45
	5	118.6	-46.01	-60.71	25.48
	6	141.7	-54.75	-72.79	30.51
	9	209.8	-80.35	-108.7	45.37
	10	232.3	-88.53	-120.8	50.35
	11	254.7	-96.62	-133.0	55.32

formation of bursts in an instrument and frequency-specific way¹².

The optimal value of L to identify the QPO frequencies, using the theoretical value ν_{fit} (given by Eq. 10), is determined so that the value of \mathcal{F} defined as

$$\mathcal{F}(L) \equiv \sum_i \frac{(\nu_{0,i} - \nu_{\text{fit},i})^2}{\Delta\nu_{0,i}^2} \quad (13)$$

is minimized, assuming the correspondence between each pair $(\nu_{0,i}, \ell)$, obtained by identifying the i -th QPO frequency with one of the ℓ -th torsional oscillation frequencies given by $\nu_{\text{fit},i}$, in such a way that the lowest candidate frequency, i.e., 18.1 Hz, is anchored to the $\ell = 2$ fundamental torsional mode, as listed in Table 1. Accordingly, the optimal value of L for the stellar model with $1.4M_\odot$ and 12 km is obtained as 82.2 MeV for $N_s/N_d = 0$ and 83.1 MeV for $N_s/N_d = 1$, as shown in Fig. 1, where we also show the 1σ uncertainty in L with the shaded region. Since the 10 QPOs listed in Table 1 (except for 205.6 Hz) evaluated in the rest frame are identified with the various fundamental torsional oscillations using one free parameter (L), the number of degrees of freedom is 9. So, the 1σ uncertainty in L from the χ^2 statistic requires $\mathcal{F}(L) - \mathcal{F}(L_{\text{op}}) \approx 10.42$, with L_{op} being the optimal value of L . If one restricts the QPOs listed in Table 1 to those whose reported significance is larger than 3σ , the optimal value of L is almost unchanged (less than 0.1%), and

¹² For instance, optimizing for time varying epoch-to-epoch dispersion measure variations (for a repeating FRB) in a bespoke manner.

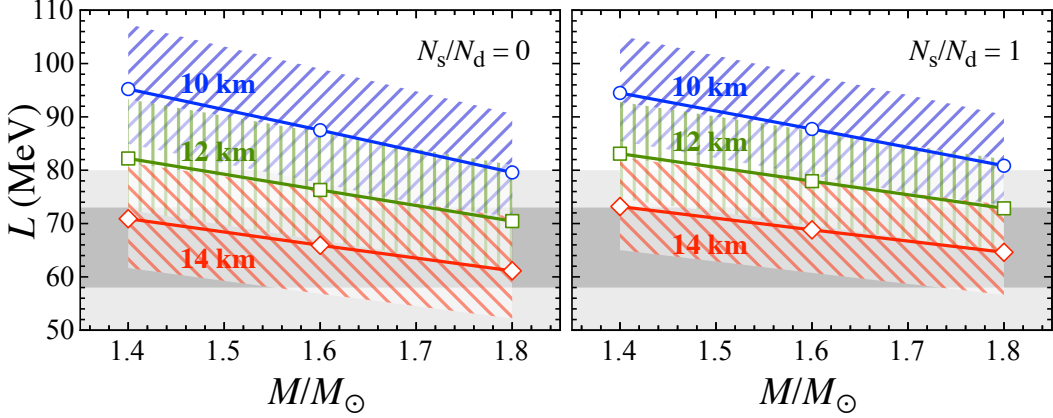


Figure 2. The optimal ranges of $L \pm 1\sigma$ to identify the observed QPO frequencies with the crustal torsional oscillations, shown for various NS models. The gray shaded regions denote the range of fiducial value of L , i.e., $L = 60 \pm 20 in light gray (M. B. Tsang et al. 2012; Newton, William G. et al. 2014; B.-A. Li et al. 2019), and the range of L constrained from the identification of magnetar QPOs observed in SGR 1806-20 with crustal torsional oscillations, i.e., $L = 58 - 73 in dark gray (H. Sotani et al. 2018; H. Sotani 2024).$$

the maximum (minimum) value of L within the $\pm 1\sigma$ range becomes at most around 4% smaller (larger). For $\tau = 3$ ms, the minimum and maximum values of L within $\pm 1\sigma$ are 72.5 and 93.3 MeV (74.6 and 92.8 MeV) for $N_s/N_d = 0$ ($N_s/N_d = 1$) via Eq. (12). With $\tau = 1.5$ ms, these values are 77.2 and 87.5 MeV (78.7 and 87.8 MeV) for $N_s/N_d = 0$ ($N_s/N_d = 1$). For $\tau = 6$ ms, they are 64.0 and 106.5 MeV (67.1 and 104.5 MeV) for $N_s/N_d = 0$ ($N_s/N_d = 1$). See also Appendix A for a more extended analysis of the dependence of our results on the choice of τ .

The optimal range for L varies with the stellar mass and radius because the fundamental frequencies depend on the stellar model. In Fig. 2, we show $L \pm 1\sigma$ for several stellar models, together with the fiducial value of L obtained from experiments, i.e., $L = 60 \pm 20 (M. B. Tsang et al. 2012; Newton, William G. et al. 2014; B.-A. Li et al. 2019), and the values constrained by the identification of the magnetar QPO frequencies observed in SGR 1806-20 as crustal torsional oscillations, i.e., $L = 58 - 73 (H. Sotani et al. 2018; H. Sotani 2024) with shaded regions. From Fig. 2, we find that stellar models with a radius of 10 km and a mass less than $\sim 1.6M_\odot$ are not consistent with the fiducial value of L , irrespective of the value of N_s/N_d in the phase of the cylindrical nuclei. In addition, we find that larger values of L are favored for models with smaller radius, for fixed stellar mass.$$

4.2. Overtones

Now we turn to the higher-frequency QPO candidates shown in Table 2. These QPOs may be identified with the first overtone of the crustal torsional oscillations, which have been shown to be almost independent of ℓ , but depend on K_0 and L . This is because the overtone frequencies depend on the crust thickness (C. J. Hansen & D. F. Cioffi 1980), and the crust thickness depends on K_0 , L , and M/R (H. Sotani et al. 2017). The overtone frequencies are well characterized

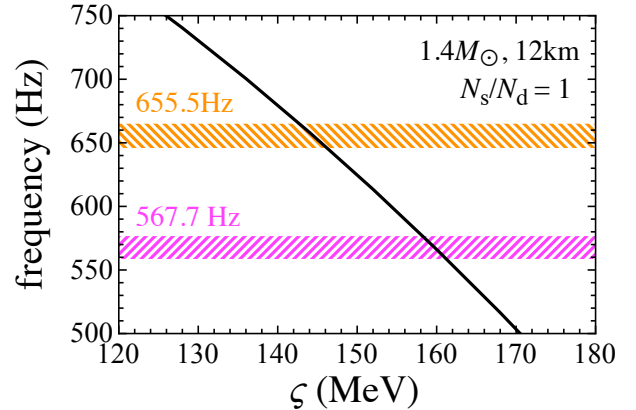


Figure 3. The ~ 600 Hz candidate QPO frequencies observed in FRB 20240114A, compared with the 1st overtone excited in a NS model with $1.4M_\odot$, 12 km, and $N_s/N_d = 1$.

by ς defined as

$$\varsigma \equiv (K_0^4 L^5)^{1/9}. \quad (14)$$

In practice, as shown in H. Sotani et al. (2018); Sotani, H. et al. (2023), the overtone frequencies of crustal torsional oscillations are expressed as a function of ς as

$$\ell t_n \text{ (Hz)} = d_{\ell n}^{(0)} + d_{\ell n}^{(1)} \varsigma_{100} + d_{\ell n}^{(2)} \varsigma_{100}^2, \quad (15)$$

where ς_{100} is defined as $\varsigma/(100 \text{ MeV})$, and $d_{\ell n}^{(i)}$ for $i = 0, 1, 2$ are fitting parameters depending on the stellar mass, radius, and N_s/N_d , but almost completely independent of ℓ . Thus, once an identification of a high-frequency QPO is made with the overtone, a constraint on ς is obtained. This constraint is independent of the constraint on L obtained through identification of the fundamental oscillations, shown in Fig. 2.

Next, we attempt to identify the frequencies listed in Table 2 except for the 301.7 and 370.8 Hz QPOs, as the 1st

Table 4. The allowed maximum and minimum masses for the NS models with 14 and 12 km and with $N_s/N_d = 0$ and 1, constrained by identifying the 567.7 Hz or 655.5 Hz QPOs with the 1st overtone of crustal oscillations and by identifying the lower QPOs with the fundamental torsional oscillations, together with the terrestrial constraint on K_0 . In addition, the value of L_{\max} (L_{\min}) corresponding to the NS model with the allowed maximum mass (minimum mass) is also listed.

QPO (Hz)	N_s/N_d	R (km)	M_{\max}/M_{\odot}	M_{\min}/M_{\odot}	L_{\max} (MeV)	L_{\min} (MeV)
567.7	0	14	1.55	1.29	77.5	64.3
		12	1.29	1.04	96.8	82.9
	1	14	1.54	1.27	79.3	67.7
		12	1.27	1.00	96.4	84.7
655.5	0	14	1.76	1.49	72.1	59.5
		12	1.46	1.19	91.5	78.4
	1	14	1.75	1.48	74.5	63.3
		12	1.44	1.17	91.7	80.5

overtone of the crustal torsional oscillations.¹³ In Fig. 3, we show as an example the comparison of the QPO frequencies with the 1st overtone as a function of ς for the stellar model with $1.4M_{\odot}$, 12 km, and $N_s/N_d = 1$, and the coefficients in Eq. (15) are $d_{\ell n}^{(0)} = 1042$, $d_{\ell n}^{(1)} = 11.48$, and $d_{\ell n}^{(2)} = -193.0$. Through the identification of the ~ 600 Hz QPO frequencies with the 1st overtone, we can obtain a constraint on ς for each stellar model. The resulting constraints on ς are shown in Fig. 4 for varying stellar mass and radius with $N_s/N_d = 0$ (top panel) or 1 (bottom panel).

We note that both 1st overtone candidates at 567.7 Hz and 655.5 Hz cannot be identified simultaneously in our non-magnetized crust formalism with different crustal torsional modes (if the reported uncertainties are not underestimated in D. Zhou et al. 2025). This is because the model overtones are almost independent of the azimuthal quantum number, ℓ , and the frequency difference between overtones is much larger than the difference between 567.7 Hz and 655.5 Hz (e.g., the frequency of the 2nd overtone is approximately 1 kHz). Since the frequency depends on the chosen (global) background model, one could simultaneously account for both frequencies if, for example, the stellar mass and/or magnetic field structures were to change. However, these two candidate QPOs are observed less than one day apart, and it is difficult to envision such significant and quick changes of the global NS field/crust structure ($\Delta M \sim \mathcal{O}(0.1M_{\odot})$ and/or $\Delta B \sim \mathcal{O}(10^{15}\text{G})$).

Accordingly, we assume that only one of the two higher-frequency QPO candidates originates from the 1st overtone, whereas the other QPO may arise from a different NS mode, such as a shear or gravity mode, or a high- ℓ fundamental

crustal torsional mode, imprinted on the signal. Therefore, we analyze each candidate overtone separately.

The combination of the constraint on L from the identification of the lower QPO frequencies with the fundamental torsional oscillations, shown in Fig. 2, and the constraint on ς from the identification of higher QPO frequency with the 1st overtone, shown in Fig. 4, gives us a constraint on K_0 via

$$K_0 = (\varsigma^9/L^5)^{1/4}. \quad (16)$$

In Fig. 5 we present our constraint on K_0 , together with the fiducial value of K_0 from experiments, $K_0 = 240 \pm 20$ MeV (S. Shlomo et al. 2006). The upper (lower) bound of K_0 in Fig. 5 comes from the upper (lower) bound of ς in Fig. 4 and the lower (upper) bound of L in Fig. 2 for each stellar model. The resulting ranges for K_0 , obtained by the identification of the QPOs with crustal torsional oscillations, can be compared with the values from experiments, and used to constrain the NS models.

In practice, focusing on the stellar models with 14 and 12 km, we obtain the maximum and minimum masses to identify the 567.7 Hz or 655.5 Hz QPO with the 1st overtone. The resulting masses for $N_s/N_d = 0$ or 1 are listed in Table 4, where the masses smaller than $1.4M_{\odot}$ are estimated by extrapolating the regions shown in Fig. 5. For a fixed stellar radius, the maximum and minimum masses constrained with $N_s/N_d = 0$ become a little larger than those with $N_s/N_d = 1$ for both cases with 567.7 and 655.5 Hz QPOs. Considering the uncertainties in N_s/N_d , the maximum mass constrained with $N_s/N_d = 0$ and the minimum mass with $N_s/N_d = 1$ gives us the allowed region of mass for the NS models with a fixed radius.

4.3. Mass-Radius Constraints

Following the procedure outlined above, we obtain the constraint on the mass and radius as viable NS models for FRB 20240114A, shown in Fig. 6. The shaded region with hashed lines from top left to bottom right (with hashed lines from top right to bottom left) is the allowed range obtained

¹³ The 301.7 and 370.8 Hz QPOs in Table 2 as well as the 205.6 Hz QPO in Table 1 could be considered as a result of the fundamental torsional oscillations with higher values of ℓ . However, given their comparatively low statistical significance, these identifications should be treated as tentative and would have limited weight in the overall mode assignment.

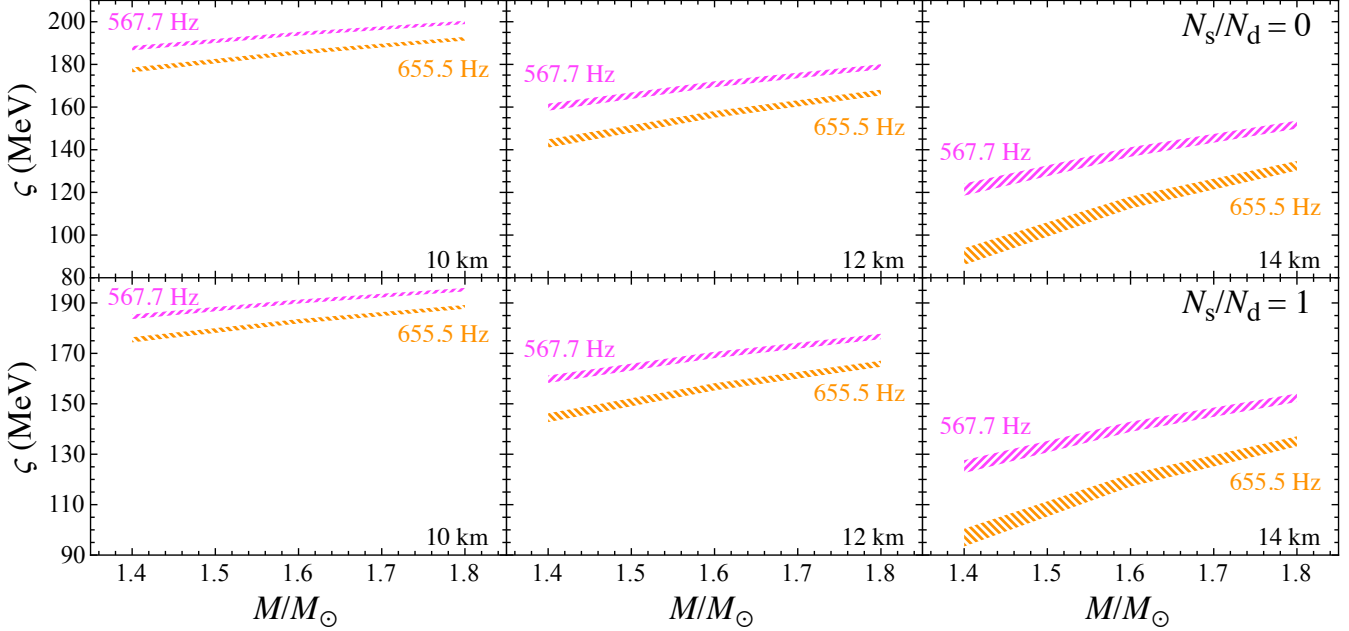


Figure 4. Constraints on the parameter ξ , obtained by identifying the QPO frequencies of ~ 600 Hz with the 1st overtone of crustal torsional oscillations. The left, middle, and right panels correspond to stellar models whose radii are 10, 12, and 14 km, respectively, while the top and bottom panels correspond to results with $N_s/N_d = 0$ and 1. In each panel, the lower and upper bounds come from the upper and lower bounds of the uncertainties in the QPO frequency (see Fig. 3).

with the identification of the 655.5 Hz (567.7 Hz) with the 1st overtone. For reference, we also plot other constraints obtained from astronomical observations, i.e., the NS mass and radius for PSR J0030+0451 (M. C. Miller et al. 2019) and PSR J0740+6620 (A. J. Dittmann et al. 2024) constrained via x-ray observations with NICER; the tidal deformability constrained by GW170817 (B. P. Abbott et al. 2017), which leads to the constraint on the $1.4M_\odot$ NS radius being $\lesssim 13.6$ km (E. Annala et al. 2018); the estimated mass and radius by identifying the magnetar higher QPOs from GRB 200415A (Sotani, H. et al. 2023); the 1σ and 2σ radius constraints, for neutron star masses between 1.4 and $2.1M_\odot$, obtained by identifying the kHz QPOs from short GRBs 910711 and 931101B (C. Chirenti et al. 2023) with the quasi-radial and quadrupolar oscillations of a binary neutron star merger remnant (V. Guedes et al. 2025), and observations of x-ray bursts (A. W. Steiner et al. 2013). The top-left shaded region is excluded by causality (J. M. Lattimer 2012), while the bottom-right shaded region denotes the NS mass and radius estimated from the fiducial values of the nuclear saturation parameters, i.e., $K_0 = 240 \pm 20$ MeV and $L = 60 \pm 20$ MeV, using the mass formula for a low-mass NS discussed in the next paragraph (H. Sotani et al. 2014). Additionally, the mass and radius for NS models constructed with several realistic EOS are shown with solid and dashed lines.

In Fig. 6, the filled circle and filled square (filled diamond and filled triangle) denote the NS models with the lowest mass with 14 km and 12 km radius, respectively, obtained by identifying the 655.5 Hz (567.7 Hz) QPO with the 1st over-

tone of crustal torsional oscillations. Each of these points should be connected, through a series of equilibrium models, to the corresponding limit provided by the low-density EOS, which can be obtained as follows. H. Sotani et al. (2014) suggest that the mass and gravitational redshift for low-mass NS models, whose central density is less than twice the nuclear saturation density, are well expressed as a function of the central density and a combination of the nuclear saturation parameters defined as

$$\eta \equiv (K_0 L^2)^{1/3}. \quad (17)$$

Using the relations provided by H. Sotani et al. (2014), we can estimate the mass and radius for low-mass NS models. We find that the mass for a NS model with fixed L (central density) increases as the central density (L) increases, which leads to L increasing with radius. This trend is opposite to the result obtained from identifying the lower QPOs with the fundamental torsional oscillations. In fact, the NS mass and radius thus estimated, using the same value of L and $K_0 = 220$ MeV for the stellar models denoted with the filled circle, filled square, filled diamond, and filled triangle (see L_{\min} in Table 4), are shown with the open circles, open squares, open diamonds, and open triangles in Fig. 6. So, for example, in a sequence of models determined by the same EOS, the stellar model denoted by the filled circle should be connected to the leftmost open circle. Therefore, we may be able to estimate the NS mass with a radius smaller than 12 km or larger than 14 km by identifying the higher QPO with the 1st overtone,

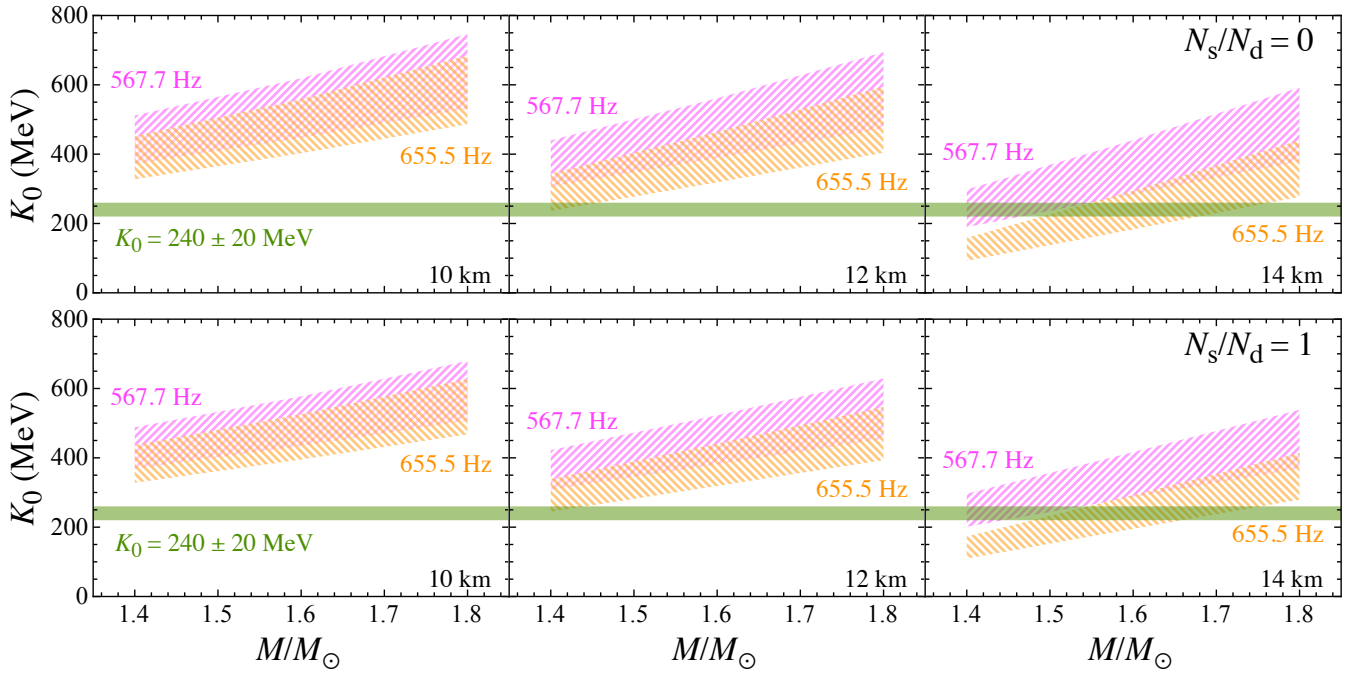


Figure 5. Constraint on K_0 obtained from the combination of the constraints on L shown in Fig. 2 and ς shown in Fig 4 by identifying the QPO frequencies with the crustal torsional oscillations. For reference, the fiducial value of K_0 obtained from the terrestrial experiments, i.e., $K_0 = 240 \pm 20$ MeV (S. Shlomo et al. 2006), is also shown.

but such a stellar model would be more difficult to connect to the lower-mass NS sequence.

Considering the necessary interpolation to the lower-mass sequence, the radius of the NS model for FRB 20240114A is ~ 13 km. A possible sequence of low-mass NSs with $L = 74$ MeV (the median value for the stellar models shown with open diamonds and squares), is shown in Fig. 6 with the solid black line, and it is naturally connected to the allowed region that we constrained in this study. As an illustrative example, we extend this sequence with the dotted line, which has a fixed stellar radius ($R = 12.9$ km). In more general cases, the dotted line curves left or right, depending on the EOS. A very sharp turn left or right is not expected in realistic EOS, and thus the data limits the viable self-consistent range of the radius to be around ~ 13 km.

Our results also provide constraints on the value of L . Whereas in Fig. 6 we focus on the mass constraints for stellar models with a given radius, in Fig. 7 we show the corresponding constraints on L , given in Table 4. We also show the fiducial value of L , i.e., $L = 60 \pm 20$ MeV (from experiments), as well as the constraint obtained from the identification of magnetar QPOs by H. Sotani et al. (2018); H. Sotani (2024), i.e., 58 – 73 MeV. The allowed values of L obtained from this study are in the range of $L = 59.5 – 96.8$ MeV, which is broadly consistent with the fiducial value of L and also with the constraint from the magnetar QPOs. Since this allowed range of L depends on the stellar mass (and radius), it would become more restrictive if constraints on the mass and/or radius of the source (FRB 20240114A) were obtained through other observations.

5. CONCLUSION

FRBs are energetic phenomena that we observe mostly from extragalactic distances. The QPOs recently discovered in FRB 20240114A motivate our systematic study of the crustal torsional oscillations that can be excited in a NS. The lower-frequency QPOs can be identified with the fundamental oscillations with various azimuthal quantum numbers, enabling us to constrain the density dependence of the nuclear symmetry energy slope parameter, L . On the other hand, the higher-frequency QPO is considered as a result of the 1st overtone, and its identification leads to another constraint on the combination of the nuclear saturation parameters, $\varsigma = (K_0^4 L^5)^{1/9}$. This constraint on ς together with the constraint on L , obtained from the identification of the lower QPOs, produces a constraint on the incompressibility coefficient K_0 , depending on the stellar model. However, K_0 is constrained by various terrestrial experiments, which prove to be more stringent than the constraint obtained in this study. That is, the experimental constraint on K_0 can select the stellar models consistent with this interpretation for the QPOs.

We caution, however, that if the observed QPOs are related to magneto-elastic oscillations (i.e., not purely crustal), then a mapping to non-magnetic crust modes can become systematically biased. The inferred L and the inferred M - R region could shift or widen substantially.

Finally, even if some individual radio QPOs are of marginal statistical significance, in aggregate they may be significant. This can only be tested by future large samples and families of FRB QPOs, or strong harmonic clus-

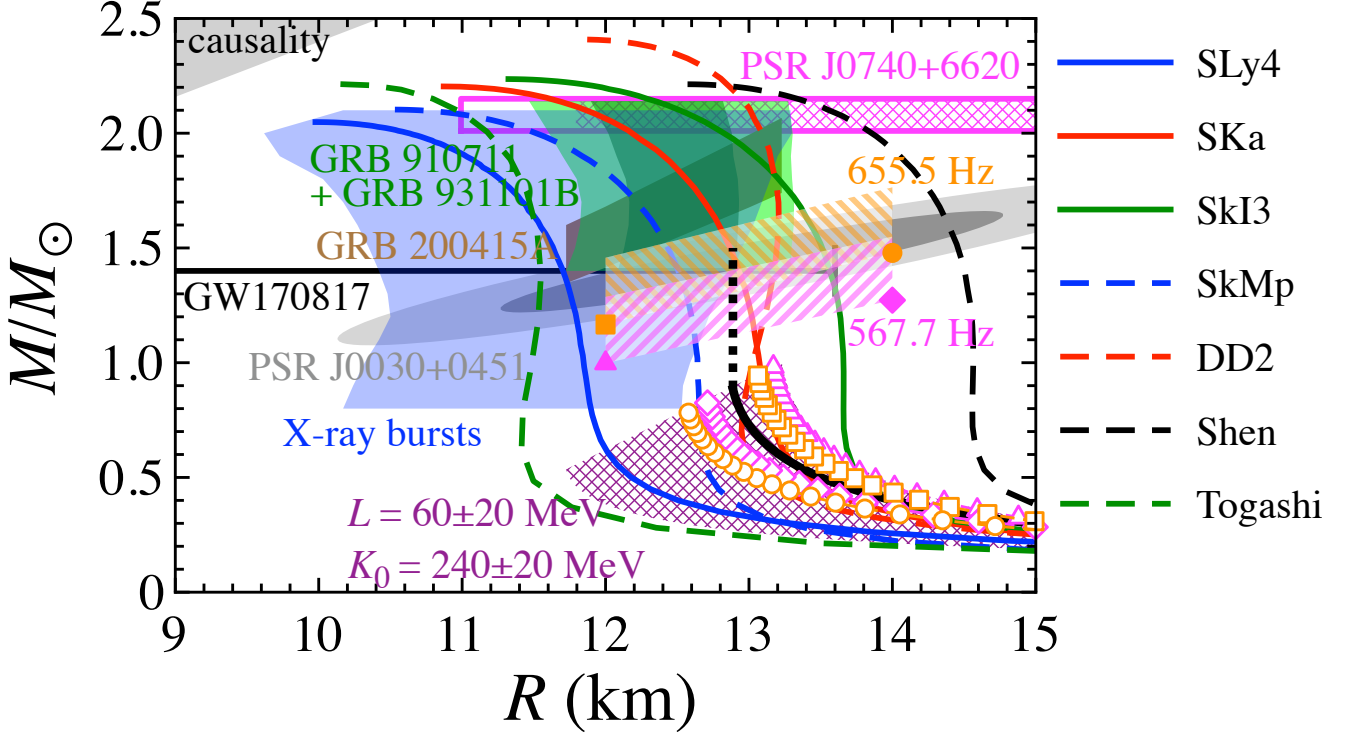


Figure 6. The mass and radius of FRB 20240114A, constrained from the identification of the QPO frequencies with the crustal torsional oscillations, together with the constraint on the nuclear parameter obtained from the terrestrial experiments, are shown with the shaded regions with hashed lines, where the shaded region with hashed lines from top left to bottom right (with hashed lines from top right to bottom left) is the allowed region with the identification of the 655.5 Hz (567.7 Hz) with the 1st overtone. The sequences with open circles, open squares, open diamonds, and open triangles denote the NS mass and radius estimated from the low-mass formula (H. Sotani et al. 2014), using the same values of L and K_0 for the stellar models marked with the filled circle, filled square, filled diamond, and filled triangle, respectively. For reference, we also show the other astronomical constraints on the NS mass and radius for PSR J0030+0451, PSR J0740+6620, GW170817, GRB 200415A, a combination of GRB 910711 and GRB 931101B and x-ray bursts; the theoretical constraint from causality; and the expected mass and radius from the fiducial values of L and K_0 constrained from the experiments (see text for details). In addition, the stellar models shown with a black solid line are the low-mass NS sequence, assuming $L = 74$ MeV, which is a median value for the stellar models shown with open diamonds and squares, while the black dotted line is just an extension of the black solid line by fixing the radius ($R = 12.9$ km).

tering in FRB short waiting time distributions, over a broad range of cosmological redshifts. This may be feasible with DSA (G. Hallinan et al. 2019) and CHORD (K. Vanderlinde et al. 2019). If QPO-like periodicities are confirmed in multiple repeaters, the field is likely to shift from single-source inversions to population-based seismology, constraining EOS parameters (assuming there is a single EOS that describes cold dense matter) statistically across sources. We note that the remarkably consistent results we have obtained from a mapping to non-magnetic crustal modes suggest either global fields lower than $\text{few} \times 10^{15}$ G or perhaps stronger core-confined fields with only a limited region of active crust field evolution (e.g., S. K. Lander 2024; S. K. Lander et al. 2026) powering activity. In the end, why particular individual modes are preferentially excited, imprinted (e.g., L. Bur naz et al. 2025) or observationally recoverable over others is an open question, which may be source, geometry or crust perturbation specific even without instrumentation selection

biases. We note that the hard X-ray giant flare tail of SGR 1806-20 also exhibits clustering of transient frequencies with observability biased by rotational phase (M. C. Miller et al. 2019).

ACKNOWLEDGMENTS

This work is supported in part by the Japan Society for the Promotion of Science (JSPS) KAKENHI Grant Numbers JP23K20848 and JP24KF0090. The material is based upon work supported by NASA under award numbers 80GSFC21M0002 and 80GSFC24M0006. We thank Paz Beniamini and Cole Miller for interesting discussions and Victor Guedes for sharing the data from the analysis of the BATSE QPOs. This work has made use of the NASA Astrophysics Data System.

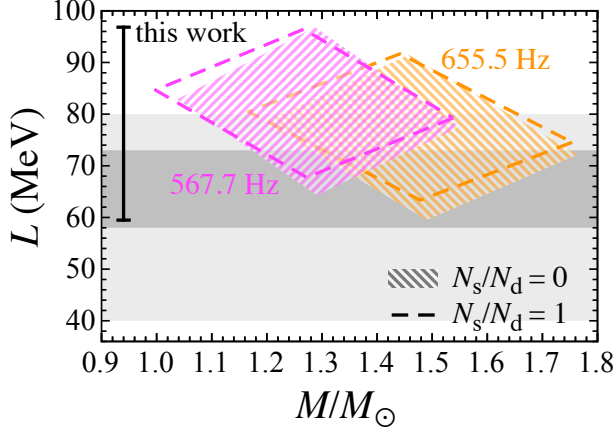


Figure 7. Constraint on L obtained by identifying the QPO frequencies with crustal torsional oscillations, together with the experimental constraint on K_0 . The shaded region with hashed lines and the region enclosed by the dashed line denote the constraints on L , for stellar models with $N_s/N_d = 0$ and 1, respectively. From our analysis, we find $L = 59.5 - 96.8$ MeV. The fiducial value of L from experiments, $L = 60 \pm 20$ MeV (M. B. Tsang et al. 2012; Newton, William G. et al. 2014; B.-A. Li et al. 2019), and the constraint obtained from the analysis of magnetar QPOs, $L = 58 - 73$ MeV (H. Sotani et al. 2018; H. Sotani 2024), are also shown with the light and dark gray shaded regions, respectively.

APPENDIX

A. DEPENDENCE OF THE FINAL RESULTS ON THE SELECTION OF τ

As in Table 4, Tables 5 and 6 list the allowed ranges of maximum and minimum masses for the NS models with 14 and 12 km and with $N_s/N_d = 0$ and 1, but with $\tau = 1.5$ ms and $\tau = 6$ ms, respectively. These results are obtained by identifying 567.7 or 655.5 Hz QPOs with the 1st overtone of crustal torsional oscillations and by identifying the lower QPOs with the fundamental oscillations with various ℓ , incorporating experimental constraints on K_0 . The corresponding bounds on L , L_{\max} and L_{\min} , are also listed. In both tables, the bracketed numbers following each entry denote the fractional deviation from the corresponding value for $\tau = 3.0$ ms (shown in Table 4). The allowed maximum and minimum masses vary by a few % with $\tau = 1.5$ ms, see Table 5; the allowed maximum (minimum) masses vary by up to 18% (a few %) with $\tau = 6.0$ ms, see Table 6.

As a result, doubling or halving the uncertainty τ results in $\lesssim 10\%$ changes in most cases. The NS mass ranges obtained from the identification of the 567.7 or 655.5 Hz QPOs with the 1st overtone become, respectively, $1.02 - 1.50 M_\odot$ or $1.19 - 1.71 M_\odot$ with $\tau = 1.5$ ms and $0.96 - 1.66 M_\odot$ or $1.12 - 2.08 M_\odot$ with $\tau = 6.0$ ms. Meanwhile, the constraint on L from the optimal stellar models for explaining the QPO observations in FRB 20240114A with $\tau = 1.5$ or 6.0 ms, obtained when plotted as shown in Fig. 7 becomes respectively $L = 63.2 - 92.5$ MeV with $\tau = 1.5$ ms and $L = 52.6 - 106.5$ MeV with $\tau = 6.0$ ms.

REFERENCES

Abbott, B. P., Abbott, R., Abbott, T. D., et al. 2017, Phys. Rev. Lett., 119, 161101, doi: [10.1103/PhysRevLett.119.161101](https://doi.org/10.1103/PhysRevLett.119.161101) 4.3

Andersson, N., & Kokkotas, K. D. 1996, Phys. Rev. Lett., 77, 4134, doi: [10.1103/PhysRevLett.77.4134](https://doi.org/10.1103/PhysRevLett.77.4134) 1

Andersson, N., & Kokkotas, K. D. 1998, Monthly Notices of the Royal Astronomical Society, 299, 1059, doi: [10.1046/j.1365-8711.1998.01840.x](https://doi.org/10.1046/j.1365-8711.1998.01840.x) 1

Annala, E., Gorda, T., Kurkela, A., & Vuorinen, A. 2018, Phys. Rev. Lett., 120, 172703, doi: [10.1103/PhysRevLett.120.172703](https://doi.org/10.1103/PhysRevLett.120.172703) 4.3

Table 5. Same as Table 4, but with $\tau = 1.5$ ms. The values in the bracket next to each entry indicate the relative deviation from the value when $\tau = 3.0$ ms (c.f. Table 4).

QPO (Hz)	N_s/N_d	R (km)	M_{\max}/M_{\odot}	M_{\min}/M_{\odot}	L_{\max} (MeV)	L_{\min} (MeV)
567.7	0	14	1.50 (3.02%)	1.32 (2.08%)	73.4 (5.37%)	68.2 (6.02%)
		12	1.24 (3.58%)	1.06 (2.13%)	92.4 (4.62%)	87.1 (5.09%)
	1	14	1.49 (2.90%)	1.30 (2.10%)	75.6 (4.67%)	71.2 (5.05%)
		12	1.22 (3.66%)	1.02 (2.36%)	92.5 (4.08%)	88.3 (4.31%)
655.5	0	14	1.71 (2.81%)	1.52 (2.09%)	68.1 (5.60%)	63.2 (6.20%)
		12	1.41 (3.32%)	1.22 (2.22%)	87.3 (4.64%)	82.4 (5.11%)
	1	14	1.71 (2.69%)	1.51 (1.99%)	70.9 (4.84%)	66.7 (5.24%)
		12	1.39 (3.27%)	1.19 (2.30%)	87.9 (4.11%)	84.0 (4.36%)

Table 6. Same as Table 4, but with $\tau = 6.0$ ms. The values in the bracket next to each entry indicate the relative deviation from the value when $\tau = 3.0$ ms (c.f. Table 4).

QPO (Hz)	N_s/N_d	R (km)	M_{\max}/M_{\odot}	M_{\min}/M_{\odot}	L_{\max} (MeV)	L_{\min} (MeV)
567.7	0	14	1.66 (7.13%)	1.25 (3.45%)	86.5 (11.6%)	57.0 (11.3%)
		12	1.40 (8.86%)	1.00 (3.17%)	106.5 (10.0%)	74.9 (9.62%)
	1	14	1.64 (6.78%)	1.23 (3.57%)	87.3 (10.1%)	61.3 (9.55%)
		12	1.38 (9.01%)	0.961 (3.65%)	105.1 (8.95%)	77.8 (8.13%)
655.5	0	14	2.08 (17.6%)	1.44 (3.65%)	77.7 (7.68%)	52.6 (11.6%)
		12	1.57 (8.00%)	1.15 (3.58%)	100.6 (9.98%)	70.9 (9.65%)
	1	14	1.86 (6.25%)	1.43 (3.52%)	82.3 (10.4%)	57.1 (9.89%)
		12	1.55 (7.82%)	1.12 (3.80%)	99.8 (8.91%)	73.9 (8.20%)

Antoniadis, J., Freire, P. C. C., Wex, N., et al. 2013, Science, 340, 1233232, doi: [10.1126/science.1233232](https://doi.org/10.1126/science.1233232)

Beloborodov, A. M. 2017, ApJL, 843, L26, doi: [10.3847/2041-8213/aa78f3](https://doi.org/10.3847/2041-8213/aa78f3)

Beloborodov, A. M. 2020, ApJ, 896, 142, doi: [10.3847/1538-4357/ab83eb](https://doi.org/10.3847/1538-4357/ab83eb)

Beniamini, P., & Kumar, P. 2020, MNRAS, 498, 651, doi: [10.1093/mnras/staa2489](https://doi.org/10.1093/mnras/staa2489)

Beniamini, P., & Kumar, P. 2025, ApJ, 982, 45, doi: [10.3847/1538-4357/adb8e6](https://doi.org/10.3847/1538-4357/adb8e6)

Beniamini, P., Wadiasingh, Z., Hare, J., et al. 2023, MNRAS, 520, 1872, doi: [10.1093/mnras/stad208](https://doi.org/10.1093/mnras/stad208)

Beniamini, P., Wadiasingh, Z., & Metzger, B. D. 2020, MNRAS, 496, 3390, doi: [10.1093/mnras/staa1783](https://doi.org/10.1093/mnras/staa1783)

Beniamini, P., Wadiasingh, Z., Trigg, A., et al. 2025, ApJ, 980, 211, doi: [10.3847/1538-4357/ada947](https://doi.org/10.3847/1538-4357/ada947)

Bethapudi, S., Li, D. Z., Spitler, L. G., et al. 2025, A&A, 702, A248, doi: [10.1051/0004-6361/202556347](https://doi.org/10.1051/0004-6361/202556347)

Bhardwaj, M., Kirichenko, A., & Gil de Paz, A. 2024, The Astronomer's Telegram, 16613, 1

Bhardwaj, M., Snelders, M. P., Hessels, J. W. T., et al. 2025, ApJL, 992, L35, doi: [10.3847/2041-8213/ae0b68](https://doi.org/10.3847/2041-8213/ae0b68)

Bilous, A. V., van Leeuwen, J., Maan, Y., et al. 2025, A&A, 696, A194, doi: [10.1051/0004-6361/202451413](https://doi.org/10.1051/0004-6361/202451413)

Bochenek, C. D., Ravi, V., Belov, K. V., et al. 2020, Nature, 587, 59, doi: [10.1038/s41586-020-2872-x](https://doi.org/10.1038/s41586-020-2872-x)

Bretz, J., van Eysden, A., & Link, B. 2017, in APS Meeting Abstracts, Vol. 2017, APS April Meeting Abstracts, Y4.007

Bretz, J., van Eysden, C. A., & Link, B. 2021, MNRAS, 504, 5880, doi: [10.1093/mnras/stab1220](https://doi.org/10.1093/mnras/stab1220)

Bruni, G., Piro, L., Yang, Y.-P., et al. 2025, A&A, 695, L12, doi: [10.1051/0004-6361/202453233](https://doi.org/10.1051/0004-6361/202453233)

Burnaz, L., Most, E. R., & Bransgrove, A. 2025, ApJL, 995, L57, doi: [10.3847/2041-8213/ae2466](https://doi.org/10.3847/2041-8213/ae2466)

Caleb, M., & Keane, E. 2021, Universe, 7, 453, doi: [10.3390/universe7110453](https://doi.org/10.3390/universe7110453)

Chamel, N. 2012, Phys. Rev. C, 85, 035801, doi: [10.1103/PhysRevC.85.035801](https://doi.org/10.1103/PhysRevC.85.035801)

Chen, X.-L., Tsai, C.-W., Li, D., et al. 2025, The Host Galaxy of the Hyperactive Repeating FRB 20240114A: Behind a Galaxy Cluster, <https://arxiv.org/abs/2502.05587> 2

CHIME/FRB Collaboration, Andersen, B. C., Bandura, K. M., et al. 2020, Nature, 587, 54, doi: [10.1038/s41586-020-2863-y](https://doi.org/10.1038/s41586-020-2863-y) 1

CHIME/FRB Collaboration, Andersen, B. C., Bandura, K., et al. 2022, Nature, 607, 256, doi: [10.1038/s41586-022-04841-8](https://doi.org/10.1038/s41586-022-04841-8) 1

Chirenti, C., Dichiara, S., Lien, A., Miller, M. C., & Preece, R. 2023, Nature, 613, 253, doi: [10.1038/s41586-022-05497-0](https://doi.org/10.1038/s41586-022-05497-0) 4.3

Cooper, A. J., & Wadiasingh, Z. 2024, MNRAS, 533, 2133, doi: [10.1093/mnras/stae1813](https://doi.org/10.1093/mnras/stae1813) 1

Crawford, F., Hisano, S., Golden, M., et al. 2022, MNRAS, 515, 3698, doi: [10.1093/mnras/stac2101](https://doi.org/10.1093/mnras/stac2101) 1

Cromartie, H. T., Fonseca, E., Ransom, S. M., et al. 2020, Nature Astronomy, 4, 72, doi: [10.1038/s41550-019-0880-2](https://doi.org/10.1038/s41550-019-0880-2) 1

de Souza, G. H., & Chirenti, C. 2019, PhRvD, 100, 043017, doi: [10.1103/PhysRevD.100.043017](https://doi.org/10.1103/PhysRevD.100.043017) 1

Demorest, P. B., Pennucci, T., Ransom, S. M., Roberts, M. S. E., & Hessels, J. W. T. 2010, Nature, 467, 1081, doi: [10.1038/nature09466](https://doi.org/10.1038/nature09466) 1

Dial, T., Deller, A. T., Uttarkar, P. A., et al. 2025, MNRAS, 536, 3220, doi: [10.1093/mnras/stae2756](https://doi.org/10.1093/mnras/stae2756) 1

Dittmann, A. J., Miller, M. C., Lamb, F. K., et al. 2024, ApJ, 974, 295, doi: [10.3847/1538-4357/ad5f1e](https://doi.org/10.3847/1538-4357/ad5f1e) 4.3

Doneva, D. D., Gaertig, E., Kokkotas, K. D., & Krüger, C. 2013, Phys. Rev. D, 88, 044052, doi: [10.1103/PhysRevD.88.044052](https://doi.org/10.1103/PhysRevD.88.044052) 1

Fonseca, E., Cromartie, H. T., Pennucci, T. T., et al. 2021, ApJL, 915, L12, doi: [10.3847/2041-8213/ac03b8](https://doi.org/10.3847/2041-8213/ac03b8) 1

Gabler, M., Cerdá-Durán, P., Font, J. A., Müller, E., & Stergioulas, N. 2013, Monthly Notices of the Royal Astronomical Society, 430, 1811, doi: [10.1093/mnras/sts721](https://doi.org/10.1093/mnras/sts721) 1

Gabler, M., Cerdá-Durán, P., Stergioulas, N., Font, J. A., & Müller, E. 2018, Monthly Notices of the Royal Astronomical Society, 476, 4199, doi: [10.1093/mnras/sty445](https://doi.org/10.1093/mnras/sty445) 1

Ge, M. Y., Liu, C. Z., Zhang, S. N., et al. 2023, ApJ, 953, 67, doi: [10.3847/1538-4357/acda1d](https://doi.org/10.3847/1538-4357/acda1d) 1

Gearheart, M., Newton, W. G., Hooker, J., & Li, B.-A. 2011, Monthly Notices of the Royal Astronomical Society, 418, 2343, doi: [10.1111/j.1365-2966.2011.19628.x](https://doi.org/10.1111/j.1365-2966.2011.19628.x) 1

Giri, U., Andersen, B. C., Chawla, P., et al. 2023, arXiv e-prints, arXiv:2310.16932, doi: [10.48550/arXiv.2310.16932](https://doi.org/10.48550/arXiv.2310.16932) 1

Guedes, V., Radice, D., Chirenti, C., & Yagi, K. 2025, The Astrophysical Journal, 983, 88, doi: [10.3847/1538-4357/adc101](https://doi.org/10.3847/1538-4357/adc101) 4.3

Hallinan, G., Ravi, V., Weinreb, S., et al. 2019, in Bulletin of the American Astronomical Society, Vol. 51, 255, doi: [10.48550/arXiv.1907.07648](https://doi.org/10.48550/arXiv.1907.07648) 1, 5

Hansen, C. J., & Cioffi, D. F. 1980, ApJ, 238, 740, doi: [10.1086/158031](https://doi.org/10.1086/158031) 4.2

Hessels, J. W. T., Spitler, L. G., Seymour, A. D., et al. 2019, ApJL, 876, L23, doi: [10.3847/2041-8213/ab13ae](https://doi.org/10.3847/2041-8213/ab13ae) 1

Hu, C.-P., Narita, T., Enoto, T., et al. 2024, Nature, 626, 500, doi: [10.1038/s41586-023-07012-5](https://doi.org/10.1038/s41586-023-07012-5) 1

Hu, C.-P., Wadiasingh, Z., Ho, W. C. G., et al. 2025, ApJ, 989, 63, doi: [10.3847/1538-4357/adea4e](https://doi.org/10.3847/1538-4357/adea4e) 1

Huppenkothen, D., Heil, L. M., Watts, A. L., & Göğüş, E. 2014a, ApJ, 795, 114, doi: [10.1088/0004-637X/795/2/114](https://doi.org/10.1088/0004-637X/795/2/114) 1

Huppenkothen, D., D'Angelo, C., Watts, A. L., et al. 2014b, ApJ, 787, 128, doi: [10.1088/0004-637X/787/2/128](https://doi.org/10.1088/0004-637X/787/2/128) 1

Huppenkothen, D., Brewer, B. J., Hogg, D. W., et al. 2015, ApJ, 810, 66, doi: [10.1088/0004-637X/810/1/66](https://doi.org/10.1088/0004-637X/810/1/66) 1

Jahns, J. N., Spitler, L. G., Nimmo, K., et al. 2023, MNRAS, 519, 666, doi: [10.1093/mnras/stac3446](https://doi.org/10.1093/mnras/stac3446) 1

Katz, J. I. 2025, arXiv e-prints, arXiv:2512.24936, doi: [10.48550/arXiv.2512.24936](https://doi.org/10.48550/arXiv.2512.24936) 1

Kramer, M., Liu, K., Desvignes, G., Karuppusamy, R., & Stappers, B. W. 2024, Nature Astronomy, 8, 230, doi: [10.1038/s41550-023-02125-3](https://doi.org/10.1038/s41550-023-02125-3) 1

Kumar, A., Maan, Y., Lal, B., et al. 2025, arXiv e-prints, arXiv:2512.21889, doi: [10.48550/arXiv.2512.21889](https://doi.org/10.48550/arXiv.2512.21889) 1

Kumar, P., Lu, W., & Bhattacharya, M. 2017, MNRAS, 468, 2726, doi: [10.1093/mnras/stx665](https://doi.org/10.1093/mnras/stx665) 1

Lander, S. K. 2024, MNRAS, 535, 2449, doi: [10.1093/mnras/stae2453](https://doi.org/10.1093/mnras/stae2453) 5

Lander, S. K., Gourgouliatos, K. N., Wadiasingh, Z., & Antonopoulou, D. 2026, The Astrophysical Journal Letters, 997, L7, doi: [10.3847/2041-8213/ae31f5](https://doi.org/10.3847/2041-8213/ae31f5) 1, 5

Lattimer, J. M. 2012, Annual Review of Nuclear and Particle Science, 62, 485, doi: <https://doi.org/10.1146/annurev-nucl-102711-095018> 3, 4.3

Li, B.-A., Krastev, P. G., Wen, D.-H., & Zhang, N.-B. 2019, Eur. Phys. J. A, 55, 117, doi: [10.1140/epja/i2019-12780-8](https://doi.org/10.1140/epja/i2019-12780-8) 3, 2, 4.1, 7

Li, C. K., Lin, L., Xiong, S. L., et al. 2021, Nature Astronomy, 5, 378, doi: [10.1038/s41550-021-01302-6](https://doi.org/10.1038/s41550-021-01302-6) 1

Li, X., Ge, M., Lin, L., et al. 2022, ApJ, 931, 56, doi: [10.3847/1538-4357/ac6587](https://doi.org/10.3847/1538-4357/ac6587) 1

Link, B., & van Eysden, C. A. 2016a, ApJL, 823, L1, doi: [10.3847/2041-8205/823/1/L1](https://doi.org/10.3847/2041-8205/823/1/L1) 1

Link, B., & van Eysden, C. A. 2016b, ApJS, 224, 6, doi: [10.3847/0067-0049/224/1/6](https://doi.org/10.3847/0067-0049/224/1/6) 1

Linscott, I. R., & Erkes, J. W. 1980, ApJL, 236, L109, doi: [10.1086/183209](https://doi.org/10.1086/183209) 1

Lorimer, D. R., Bailes, M., McLaughlin, M. A., Narkevic, D. J., & Crawford, F. 2007, Science, 318, 777, doi: [10.1126/science.1147532](https://doi.org/10.1126/science.1147532) 1

Lorimer, D. R., McLaughlin, M. A., & Bailes, M. 2024, Ap&SS, 369, 59, doi: [10.1007/s10509-024-04322-6](https://doi.org/10.1007/s10509-024-04322-6) 1

Lyubarsky, Y. 2014, MNRAS, 442, L9, doi: [10.1093/mnrasl/slu046](https://doi.org/10.1093/mnrasl/slu046)

Lyutikov, M. 2021, ApJ, 922, 166, doi: [10.3847/1538-4357/ac1b32](https://doi.org/10.3847/1538-4357/ac1b32)

Mckinven, R., Bhardwaj, M., Eftekhari, T., et al. 2025, Nature, 637, 43, doi: [10.1038/s41586-024-08184-4](https://doi.org/10.1038/s41586-024-08184-4)

Mereghetti, S., Savchenko, V., Ferrigno, C., et al. 2020, ApJL, 898, L29, doi: [10.3847/2041-8213/aba2cf](https://doi.org/10.3847/2041-8213/aba2cf)

Metzger, B. D., Margalit, B., & Sironi, L. 2019, MNRAS, 485, 4091, doi: [10.1093/mnras/stz700](https://doi.org/10.1093/mnras/stz700)

Miller, M. C., Chirenti, C., & Strohmayer, T. E. 2019, The Astrophysical Journal, 871, 95, doi: [10.3847/1538-4357/aaf5ce](https://doi.org/10.3847/1538-4357/aaf5ce)

Miller, M. C., Lamb, F. K., Dittmann, A. J., et al. 2019, ApJL, 887, L24, doi: [10.3847/2041-8213/ab50c5](https://doi.org/10.3847/2041-8213/ab50c5)

Nan, R., Li, D., Jin, C., et al. 2011, International Journal of Modern Physics D, 20, 989, doi: [10.1142/S0218271811019335](https://doi.org/10.1142/S0218271811019335)

Newton, William G., Hooker, Joshua, Gearheart, Michael, et al. 2014, Eur. Phys. J. A, 50, 41, doi: [10.1140/epja/i2014-14041-x](https://doi.org/10.1140/epja/i2014-14041-x)

Nimmo, K., Pleunis, Z., Beniamini, P., et al. 2025, Nature, 637, 48, doi: [10.1038/s41586-024-08297-w](https://doi.org/10.1038/s41586-024-08297-w)

Niu, J.-R., Zhu, W.-W., Zhang, B., et al. 2022, Research in Astronomy and Astrophysics, 22, 124004, doi: [10.1088/1674-4527/ac995d](https://doi.org/10.1088/1674-4527/ac995d)

Niu, J. R., Wang, W. Y., Jiang, J. C., et al. 2024, ApJL, 972, L20, doi: [10.3847/2041-8213/ad7023](https://doi.org/10.3847/2041-8213/ad7023)

Oertel, M., Hempel, M., Klähn, T., & Typel, S. 2017, Rev. Mod. Phys., 89, 015007, doi: [10.1103/RevModPhys.89.015007](https://doi.org/10.1103/RevModPhys.89.015007)

Ogata, S., & Ichimaru, S. 1990, Phys. Rev. A, 42, 4867, doi: [10.1103/PhysRevA.42.4867](https://doi.org/10.1103/PhysRevA.42.4867)

Oyamatsu, K., & Iida, K. 2003, Progress of Theoretical Physics, 109, 631, doi: [10.1143/PTP.109.631](https://doi.org/10.1143/PTP.109.631)

Oyamatsu, K., & Iida, K. 2007, Phys. Rev. C, 75, 015801, doi: [10.1103/PhysRevC.75.015801](https://doi.org/10.1103/PhysRevC.75.015801)

Pastor-Marazuela, I., van Leeuwen, J., Bilous, A., et al. 2023, A&A, 678, A149, doi: [10.1051/0004-6361/20224339](https://doi.org/10.1051/0004-6361/20224339)

Pethick, C., & Potekhin, A. 1998, Physics Letters B, 427, 7, doi: [https://doi.org/10.1016/S0370-2693\(98\)00341-4](https://doi.org/10.1016/S0370-2693(98)00341-4)

Petroff, E., Hessels, J. W. T., & Lorimer, D. R. 2019, A&A Rv, 27, 4, doi: [10.1007/s00159-019-0116-6](https://doi.org/10.1007/s00159-019-0116-6)

Platts, E., Weltman, A., Walters, A., et al. 2019, PhR, 821, 1, doi: [10.1016/j.physrep.2019.06.003](https://doi.org/10.1016/j.physrep.2019.06.003)

Pleunis, Z., Good, D. C., Kaspi, V. M., et al. 2021, ApJ, 923, 1, doi: [10.3847/1538-4357/ac33ac](https://doi.org/10.3847/1538-4357/ac33ac)

Popov, S. B., & Postnov, K. A. 2010, in Evolution of Cosmic Objects through their Physical Activity, ed. H. A. Harutyunian, A. M. Mickaelian, & Y. Terzian, 129–132, doi: [10.48550/arXiv.0710.2006](https://doi.org/10.48550/arXiv.0710.2006)

Ridnaia, A., Svinkin, D., Frederiks, D., et al. 2021, Nature Astronomy, 5, 372, doi: [10.1038/s41550-020-01265-0](https://doi.org/10.1038/s41550-020-01265-0)

Romani, R. W., Kandel, D., Filippenko, A. V., Brink, T. G., & Zheng, W. 2022, Astrophys. J. Lett., 934, L17, doi: [10.3847/2041-8213/ac8007](https://doi.org/10.3847/2041-8213/ac8007)

Schumaker, B. L., & Thorne, K. S. 1983, Monthly Notices of the Royal Astronomical Society, 203, 457, doi: [10.1093/mnras/203.2.457](https://doi.org/10.1093/mnras/203.2.457)

Shapiro, S. L., & Teukolsky, S. A. 1983, Black holes, white dwarfs and neutron stars. The physics of compact objects, doi: [10.1002/9783527617661](https://doi.org/10.1002/9783527617661)

Sheikh, S. Z., Farah, W., Pollak, A. W., et al. 2024, MNRAS, 527, 10425, doi: [10.1093/mnras/stad3630](https://doi.org/10.1093/mnras/stad3630)

Sherman, M., Connor, L., Ravi, V., Law, C., & DSA-2000 Collaboration. 2024, in American Astronomical Society Meeting Abstracts, Vol. 243, American Astronomical Society Meeting Abstracts #243, 261.04

Shin, K., & CHIME/FRB Collaboration. 2024, The Astronomer's Telegram, 16420, 1

Shlomo, S., Kolomietz, V. M., & Colò, G. 2006, European Physical Journal A, 30, 23, doi: [10.1140/epja/i2006-10100-3](https://doi.org/10.1140/epja/i2006-10100-3)

Sotani, H. 2024, Universe, 10, doi: [10.3390/universe10060231](https://doi.org/10.3390/universe10060231)

Sotani, H., Iida, K., & Oyamatsu, K. 2017, Monthly Notices of the Royal Astronomical Society, 470, 4397, doi: [10.1093/mnras/stx1510](https://doi.org/10.1093/mnras/stx1510)

Sotani, H., Iida, K., & Oyamatsu, K. 2018, Monthly Notices of the Royal Astronomical Society, 479, 4735, doi: [10.1093/mnras/sty1755](https://doi.org/10.1093/mnras/sty1755)

Sotani, H., Iida, K., & Oyamatsu, K. 2019, Monthly Notices of the Royal Astronomical Society, 489, 3022, doi: [10.1093/mnras/stz2385](https://doi.org/10.1093/mnras/stz2385)

Sotani, H., Iida, K., Oyamatsu, K., & Ohnishi, A. 2014, Progress of Theoretical and Experimental Physics, 2014, 051E01, doi: [10.1093/ptep/ptu052](https://doi.org/10.1093/ptep/ptu052)

Sotani, H., Kokkotas, K. D., & Stergioulas, N. 2007, Monthly Notices of the Royal Astronomical Society, 375, 261, doi: [10.1111/j.1365-2966.2006.11304.x](https://doi.org/10.1111/j.1365-2966.2006.11304.x)

Sotani, H., Nakazato, K., Iida, K., & Oyamatsu, K. 2012a, Phys. Rev. Lett., 108, 201101, doi: [10.1103/PhysRevLett.108.201101](https://doi.org/10.1103/PhysRevLett.108.201101)

Sotani, H., Nakazato, K., Iida, K., & Oyamatsu, K. 2012b, Monthly Notices of the Royal Astronomical Society: Letters, 428, L21, doi: [10.1093/mnrasl/sls006](https://doi.org/10.1093/mnrasl/sls006)

Sotani, H., Nakazato, K., Iida, K., & Oyamatsu, K. 2013, Monthly Notices of the Royal Astronomical Society, 434, 2060, doi: [10.1093/mnras/stt1152](https://doi.org/10.1093/mnras/stt1152)

Sotani, H., Yasutake, N., Maruyama, T., & Tatsumi, T. 2011, Phys. Rev. D, 83, 024014, doi: [10.1103/PhysRevD.83.024014](https://doi.org/10.1103/PhysRevD.83.024014)

Sotani, H., Kokkotas, K. D., & Stergioulas, N. 2023, *A&A*, 676, A65, doi: [10.1051/0004-6361/202346360](https://doi.org/10.1051/0004-6361/202346360) 1, 4.2, 4.3

Steiner, A. W., Lattimer, J. M., & Brown, E. F. 2013, *ApJL*, 765, L5, doi: [10.1088/2041-8205/765/1/L5](https://doi.org/10.1088/2041-8205/765/1/L5) 4.3

Strohmayer, T., Ogata, S., Iyetomi, H., Ichimaru, S., & van Horn, H. M. 1991, *ApJ*, 375, 679, doi: [10.1086/170231](https://doi.org/10.1086/170231) 3

Strohmayer, T. E., & Watts, A. L. 2005, *ApJL*, 632, L111, doi: [10.1086/497911](https://doi.org/10.1086/497911) 1

Strohmayer, T. E., & Watts, A. L. 2006, *ApJ*, 653, 593, doi: [10.1086/508703](https://doi.org/10.1086/508703) 1

Suvorov, A. G., & Kokkotas, K. D. 2019, *MNRAS*, 488, 5887, doi: [10.1093/mnras/stz2052](https://doi.org/10.1093/mnras/stz2052) 1

Tavani, M., Casentini, C., Ursi, A., et al. 2021, *Nature Astronomy*, 5, 401, doi: [10.1038/s41550-020-01276-x](https://doi.org/10.1038/s41550-020-01276-x) 1

Thornton, D., Stappers, B., Bailes, M., et al. 2013, *Science*, 341, 53, doi: [10.1126/science.1236789](https://doi.org/10.1126/science.1236789) 1

Tian, J., Rajwade, K. M., Pastor-Marazuela, I., et al. 2024, *Monthly Notices of the Royal Astronomical Society*, 533, 3174, doi: [10.1093/mnras/stae2013](https://doi.org/10.1093/mnras/stae2013) 2

Totani, T., & Tsuzuki, Y. 2023, *MNRAS*, 526, 2795, doi: [10.1093/mnras/stad2532](https://doi.org/10.1093/mnras/stad2532) 1

Tsang, M. B., Stone, J. R., Camera, F., et al. 2012, *Phys. Rev. C*, 86, 015803, doi: [10.1103/PhysRevC.86.015803](https://doi.org/10.1103/PhysRevC.86.015803) 3, 2, 4.1, 7

Tsui, L. K., & Leung, P. T. 2005, *Monthly Notices of the Royal Astronomical Society*, 357, 1029, doi: [10.1111/j.1365-2966.2005.08710.x](https://doi.org/10.1111/j.1365-2966.2005.08710.x) 1

Vanderlinde, K., Liu, A., Gaensler, B., et al. 2019, in *Canadian Long Range Plan for Astronomy and Astrophysics White Papers*, Vol. 2020, 28, doi: [10.5281/zenodo.3765414](https://doi.org/10.5281/zenodo.3765414) 1, 5

Voisin, G. 2021, in SF2A-2021: Proceedings of the Annual meeting of the French Society of Astronomy and Astrophysics, ed. A. Siebert, K. Baillié, E. Lagadec, N. Lagarde, J. Malzac, J. B. Marquette, M. N'Diaye, J. Richard, & O. Venot, 405–412 1

Wadiasingh, Z., Beniamini, P., Timokhin, A., et al. 2020, *ApJ*, 891, 82, doi: [10.3847/1538-4357/ab6d69](https://doi.org/10.3847/1538-4357/ab6d69) 1

Wadiasingh, Z., & Chirenti, C. 2020, *The Astrophysical Journal Letters*, 903, L38, doi: [10.3847/2041-8213/abc562](https://doi.org/10.3847/2041-8213/abc562) 1, 9, 2

Wadiasingh, Z., & Timokhin, A. 2019, *ApJ*, 879, 4, doi: [10.3847/1538-4357/ab2240](https://doi.org/10.3847/1538-4357/ab2240) 1

Wang, C.-W., Xiong, S.-L., Wang, Y., et al. 2026, GECAM discovery of the second FRB-associated Magnetar X-ray Burst from SGR J1935+2154, <https://arxiv.org/abs/2602.10895> 8

Wang, W., Luo, R., Yue, H., et al. 2018, *ApJ*, 852, 140, doi: [10.3847/1538-4357/aaa025](https://doi.org/10.3847/1538-4357/aaa025) 1

Wang, W.-Y., Jiang, J.-C., Lee, K., Xu, R., & Zhang, B. 2022, *MNRAS*, 517, 5080, doi: [10.1093/mnras/stac3070](https://doi.org/10.1093/mnras/stac3070) 1

Watts, A. L., & Strohmayer, T. E. 2006, *ApJL*, 637, L117, doi: [10.1086/500735](https://doi.org/10.1086/500735) 1

Watts, A. L., & Strohmayer, T. E. 2007, *Advances in Space Research*, 40, 1446, doi: [10.1016/j.asr.2006.12.021](https://doi.org/10.1016/j.asr.2006.12.021) 1

Xiao, D., Wang, F., & Dai, Z. 2021, *Science China Physics, Mechanics, and Astronomy*, 64, 249501, doi: [10.1007/s11433-020-1661-7](https://doi.org/10.1007/s11433-020-1661-7) 1

Xiao, S., Jiang, Z.-H., & Li, D. 2026, Evidence for a Damped Millisecond Quasi-Periodic Structure in a Fast Radio Burst, <https://arxiv.org/abs/2601.03950> 1

Yamasaki, S., & Totani, T. 2025, *ApJL*, 983, L16, doi: [10.3847/2041-8213/adc10b](https://doi.org/10.3847/2041-8213/adc10b) 1

Younes, G., Güver, T., Kouveliotou, C., et al. 2020, *ApJL*, 904, L21, doi: [10.3847/2041-8213/abc94c](https://doi.org/10.3847/2041-8213/abc94c) 1

Zhang, B. 2023, *Reviews of Modern Physics*, 95, 035005, doi: [10.1103/RevModPhys.95.035005](https://doi.org/10.1103/RevModPhys.95.035005) 1

Zhang, L.-X., Tian, S., Shen, J., et al. 2025, Investigating FRB 20240114A with FAST: Morphological Classification and Drifting Rate Measurements in a Burst-Cluster Framework, <https://arxiv.org/abs/2507.14711> 1, 4.1

Zhou, D., Wang, P., Fang, J., et al. 2025, A comprehensive search for Long and Short Periodic Features from an Extremely Active Cycle of FRB 20240114A, <https://arxiv.org/abs/2507.14708> 1, 1, 2, 2, 2, 4.2